Peer-reviewed version available at *Crystals* **2018**, *8*, 398; doi:10.3390/cryst8110398

Article

High-Performance Thermal Management Nanocomposites: Silver Functionalized Graphene Nanosheets and Multiwalled Carbon Nanotube

Yongcun Zhou [1,2,*], Xiao Zhuang [1], Feixiang Wu [3,4] and Feng Liu [1,*]

[1] School of Materials Science and Engineering, Northwestern Polytechnical University, Xi'an 710072, China; zhuangxiao@mail.nwpu.edu.cn;
[2] State Key Laboratory of Electrical Insulation and Power Equipment, Xi'an Jiaotong University, Xi'an Shaanxi 710049, China
[3] School of Metallurgy and Environment, Central South University, Changsha 410083, China F.Wu@fkf.mpg.de
[4] Max Planck Institute for Solid State Research, Heisenbergstr. 1, Stuttgart 70569, Germany
* Correspondence: yczhou@nwpu.edu.cn (Y.Z.); liufeng@nwpu.edu.cn (F.L.); Tel: +86-29-8846-0374 (Y.Z. & F.L.)

Abstract: Polymer composites with high thermal conductivity have a great potential for applications in modern electronics due to their low cost, easy process, and stable physical and chemical properties. Nevertheless, most polymer composites commonly possess unsatisfactory thermal conductivity, primarily because of the high interfacial thermal resistance between inorganic fillers. Herein, we developed a novel method through silver functionalized graphene nanosheets (GNS) and multiwalled carbon nanotube (MWCNT) composites with excellent thermal properties to meet the requirements of thermal management. The effects of composites on interfacial structure and properties of the composites were identified, and the microstructures and properties of the composites were studied as a function of the volume fraction of fillers. An ultrahigh thermal conductivity of 12.3 W/mK for polymer matrix composites was obtained, which is an approximate enhancement of 69.1 times compared to the polyvinyl alcohol (PVA) matrix. Moreover, these composites showed more competitive thermal conductivities compared to untreated fillers/PVA composites applied to the desktop central processing unit, making these composites a high-performance alternative to be used for thermal management.

Keywords: chemical modification; electronics cooling; thermal management nanocomposites; thermal conductivity; silver nanoparticles

1. Introduction

Effective thermal management has become a critical issue to enhance reliability and performance in many research areas including highly integrated electronic devices, lighting components, electronics cooling, and energy-harvesting systems [1–5]. Therefore, it is essential to develop thermal management materials with high thermal conductivity (λ), low coefficient of thermal expansion (CTE), and high insulating property [1,4]. In particular, thermal interface materials (TIM) are typically composed of thermally conductive fillers and viscous polymer matrix to achieve both high thermal conductivity and good frequency stability [3–6]. TIM are essential components for efficient electronics cooling. They act by filling unavoidable air gaps between the contacting surfaces of devices and heat sinks. Carbon materials, such as graphene, carbon nanotubes (CNT), graphite, diamond, and carbon fibers (CF), have recently proved to be promising thermal management materials due to their excellent thermal properties [4–7] (graphene intrinsic thermal conductivity λ = 5300 W/mK). However, the λ of thermal management nanocomposites was not as high as expected when these

Peer-reviewed version available at Crystals 2018, 8, 398; doi:10.3390/cryst8110398

various carbon materials were embedded in various polymer matrices. This was due to the presence of an incomplete formation of thermal percolation pathway and large interfacial thermal resistance (ITR) between the fillers and polymer matrix [3–7]. The ITR could become one of the biggest obstacles for heat conduction from good-conducting fillers to poor-conducting polymers.

The ITR in polymer nanocomposites can be classified into filler/matrix resistance and filler/filler resistance [6–14]. Electrically conducting TIM with metal or nano-carbon fillers generally provide higher λ than electrically insulating TIMs with ceramic fillers because additional thermal transport could be recognized by electrons [14–17]:

$$\lambda = \lambda_e + \lambda_l = L\sigma T + \lambda_l \quad (1)$$

where λ_e is the electronic thermal conductivity, λ_l the lattice or phonon thermal conductivity, L the Lorenz number, σ the electrical conductivity, and T the absolute temperature. A significant improvement in σ of polymer matrix or composites has been observed using metal silver (Ag) fillers, nano-carbon, or their combination, approaching 40% of intrinsic σ of Ag fillers [18–23].

Herein, this study proposed an alternative simple fabrication route, which introduced silver nanoparticles (AgNPs) functionalized graphene nanosheets (GNS) and multiwalled carbon nanotube (MWCNT), forming GNS@AgNPs and MWCNT@AgNPs coating microstructures to create a silver nanoparticle "bridge", to decrease the interfacial thermal resistance between fillers. We selected GNS and MWCNT as fillers for their unique thermal conductivity compared with other materials, which are cost-effective, widely used in thermal conductive applications and in research. Meanwhile, it is more probably to obtain a 3D thermal percolation pathway through the combination of 1D and 2D fillers. We chose AgNPs as the modification materials for its similar high thermal properties, and at the same time, nanoparticles modifying increased the surface roughness of the fillers, which contributed to enhance the bonding strength between the fillers and polymer matrix and to decrease the interface resistance. (GNS-MWCNT)@AgNPs/PVA flexible film specimens were successfully prepared by introducing the aforementioned structure into a polyvinyl alcohol (PVA) matrix. This combination microstructure was designed to provide an even greater opportunity to enhance λ due to a significantly higher intrinsic λ (about 3000 W/mK) of GNS and MWCNT [23–30] than that of other high–thermal conductivity ceramic fillers, such as aluminium nitride (AlN) and boron nitride (BN). Moreover, AgNPs were chosen because of their high thermal conductivity of Ag (λ = 429 W/(mK)) [6,24]. AgNPs functionalized GNS and MWCNT showed a higher σ in functionalized fillers, forming a more effective thermally conductive network and hence, lowering the ITR effect. High thermal conductivity and good insulation performance were gained with 20 vf% low filling ratios. This TIM was successfully applied between a heat sink and a central processing unit (CPU) of the computer for efficient cooling. GNS/PVA, MWCNT/PVA and (GNS-MWCNT)/PVA specimens with the same volume fraction were prepared for comparison.

2. Materials and Methods

2.1. Materials

Ethylene glycol (EG, 99.5%), polyvinyl alcohol (PVA, powder), silver nitrate ($AgNO_3$, 99.9%), sodium chloride (NaCl, 98%), tetraethylorthosilicate (TEOS, 99.0%), and ammonium hydroxide (NH_4OH, 26 wt%) were purchased from Alfa Aesar Co. (Shanghai, China). Graphene nanosheets (GNS, about 5–9 nm in thickness and 25 μm^2 of surface area) and Multi-Walled Carbon Nanotubes (MWCNTs, 40 nm in diameter and 1–2 μm in length) were supplied by Sigma-Aldrich Company (Shanghai, China). Silver (Ag, ~50 nm) nanopowder was supplied by Beijing DK Nano Technology Co. Ltd. (Beijing, China). All other chemical reagents were used as received.

2.2. Characterization

Microstructures and morphologies of the Ag nanoparticles, GNS@AgNPs, and MWCNT@AgNPs were characterized by using a high-resolution transmission electron microscopy

(HRTEM, JEOL JEM-1230, Tokyo, Japan). The scanning electron microscopy (SEM, JEOL 7401F, Tokyo, Japan) was performed with an accelerating voltage of 10 kV, where the samples were sputter-coated with a thin layer of gold for better imaging. The thermal conductivities of the fluids were measured using Nanoflash (NETZSCH LFA 447, Bavaria, Germany) technology. In brief, the laser source emits a light pulse on the sample surface under certain temperature conditions. Consequently, the surface absorbs light energy and the temperature is instantly raised, and heat source conduction occurs towards the cold side (generally refers to the upper surface). The comprehensive thermal analysis with simultaneous differential scanning calorimetry and thermogravimetry (TG) was conducted using a thermal analyzer (NETZSCH STA449C, Bavaria, Germany). The bulk density of the specimen was measured by the water displacement method using an electronic densimeter (METTLER TOLEDO, XPE205, Greifensee, Switzerland). The resistance parameters, including volume resistivity and surface resistivity, were determined using an Agilent 4339B high-resistance meter (Agilent Technologies Japan Ltd, Tokyo, Japan) at room temperature. The specimen dimensions used to measure resistivity were prepared in the cylindrical shape of 25.4 mm in diameter and 1.0–2.0mm in thickness. The results were obtained from data average of three samples.

2.3. Preparation and Purification of GNS@AgNPs and MWCNT@AgNPs

The schematic diagram outlining the preparation of AgNPs functionalized GNS and MWCNT is shown in Figure 1; they were prepared following a previously published protocol with modifications [31–33]. GNS@AgNPs and MWCNT@AgNPs were prepared by the same procedure, which was simple and practical and could be divided into two parts.

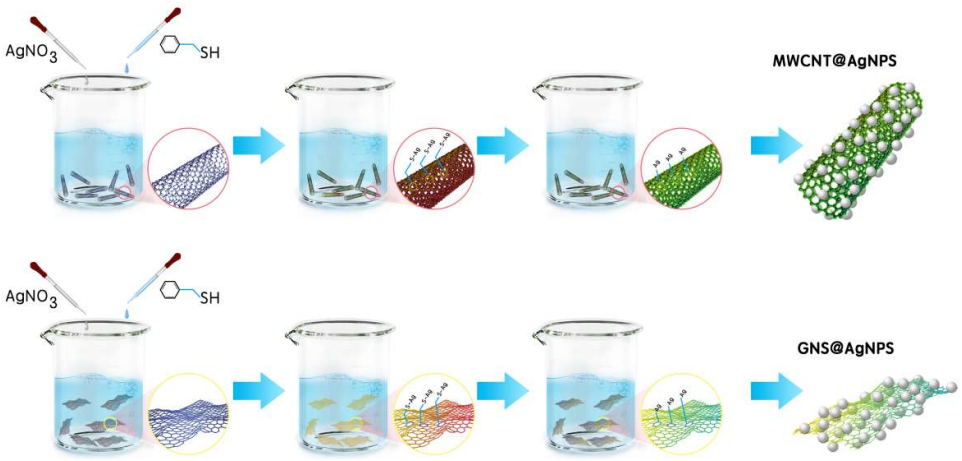

Figure 1. Schematic diagram illustrating the preparation of a coated structure of MWCNT@AgNPs and GNS@AgNPs.

(1) The synthesis of silver nanoparticles was achieved by the sol-gel method. The precursor of silver nanoparticles, silver nitrate solution in 400 mL of ethanol (0.02 mol/L), was stirred with benzyl mercaptan for about 48 h and served as a reductant. Hence, silver nanoparticles were successfully synthesized with an approximate average size of 5 nm and connected with benzyl through the ionic bond with the sulfur ion. MWCNTs with an outer diameter of 5 nm, dispersed by sonication (600W, 10 min) in ethanol were mixed with the 500 ml of silver nanoparticle solution by sonication in a bath (200W, 6 h).

(2) AgNPs and pure ultrasonically dispersed GNS or MWCNT were mixed, stirring for about 30 min, and ultrasonically shaken for about 5 h afterwards. Then, they were assembled through benzyl, the cross-linking agent, in which the sulfur ion served as a bridge between silver and benzyl because sulfur has good affinity for silver. Hence, AgNPs adhered to GNS through benzyl. As a result, GNS

Peer-reviewed version available at Crystals 2018, 8, 398; doi:10.3390/cryst8110398

and MWCNT decorated with AgNPs (GNS@AgNPs and MWCNT@AgNPs, respectively) were obtained after centrifugal separation and drying in a vacuum oven at 60 °C for about 12 h.

2.4. Preparation of GNS@AgNPs/PVA, MWCNT@AgNPs/PVA, and (GNS-MWCNT)@AgNPs/PVA

The composite film was prepared by the method of tape casting. PVA (3 g) was dissolved in deionized water to a volume of about 60 mL. Then, the dispersed GNS@AgNPs and MWCNT@AgNPs were added into the PVA solution, stirred for about 2 h, and then kept aside for 3 h to remove the bubbles formed during stirring and to facilitate the formation of a filler network across AgNPs, which was vital for the thermal conductivity of the composite. The mixture liquid was cast on the plastic film substrate and heated at 60 °C. After solidification, the cast layer was separated from the substrate artificially. Ultimately, the PVA matrix nanocomposite containing hybrid GNS@AgNPs and MWCNT@AgNPs fillers was successfully obtained.

3. Results and Discussion

The SEM and TEM images of core-shell GNS@AgNPs, MWCNT@AgNPs and 20 vol% (GNS-MWCNTs)@AgNPs/PVA film are shown in Figure 2. As shown in Figure 2a, AgNPs were uniformly attached on the surface of microscale GNS. Figure 2b shows the TEM image of AgNPs; their size was about 20 nm. Also, the silver lattice constant was about 0.23 nm, as shown in Figure 2c. Similarly, AgNPs were uniformly attached to the surface of MWCNT, as shown in Figure 2c. The silver diffraction pattern is shown in the inset of Figure 2d. As shown in Figure 2e, the thickness of composites film was about 100 μm, the highlight part inset was the fillers, (GNS-MWCNTs)@AgNPs, and the surroundings were polymer matrix. It can be seen that the fillers dispersed uniformly in the matrix and rarely agglomerate compared with the SEM images of (f), (g), and (h). This uniform distribution of fillers not only contributed to propagate phonon among fillers with high thermal conductivity but also helped to conduct 3D thermal conductive pathways in the composites. Therefore, the composites with uniform dispersion of the fillers can be obtained by this approach and the thermal conductivity of polymer composites could be enhanced as well.

The surface modification of GNS nanosheets and MWCNT by AgNPs provided hydroxyl groups on the surface of nanoparticles in the preparation process, improving the distribution of GNS-MWCNT in the PVA polymer matrix. The thermal properties of the composite films are summarized in Table 1. The pure PVA exhibited high thermal oxidation stability. The glass transition temperature (T_g) of the composite films was slightly higher than that of the pure PVA, indicating that the nanofillers increased the T_g of the PVA matrix. The thermo-oxidative decomposition behavior of the PVA nanocomposites was similar to that of PVA but showed a high decomposition temperature, suggesting that the addition of (GNS-MWCNT)/AgNPs improved the thermal stability of the PVA nanocomposites. The CTE of the composite films decreased with the increasing concentration of nanofillers. Thus, a substantial decrease in the CTE of PVA films originated from the adequate dispersion and interfacial physical bonds between the nanofillers and the PVA matrix. The nanofillers prevented the mobility of the loose molecular bonds in polymer chains with increasing temperature [33–42]. For the composite films, CTE is dependent on each component phase and the interactions between each phase. Some polymeric chains may create structures close to the nanoparticles surface, i.e., reducing the mobility of polymer segments. Since T_g is associated with the mobility of polymeric chains, less mobility results in higher T_g values. Hence, the substantial decrease in CTE of PVA films should originate from the adequate dispersion and interfacial physical bonds between the nanofillers and the PVA matrix. The nanofiller can restrain the mobility of the loose molecular bonds in polymer chains as the temperature increases.

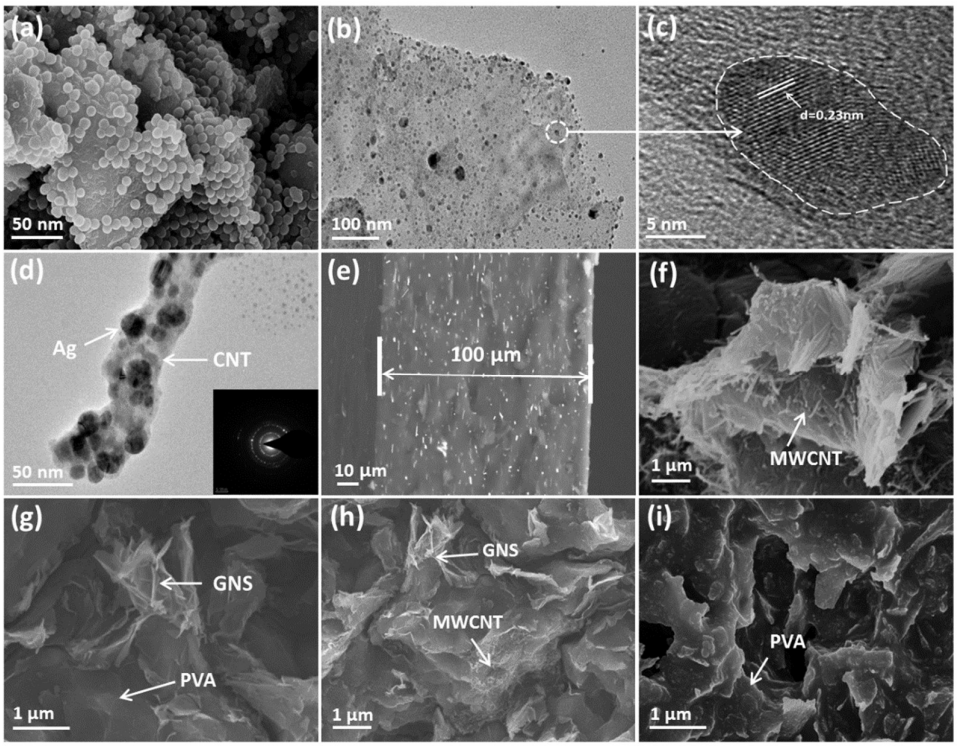

Figure 2. (**a**) SEM image of GNS@AgNPs, (**b**) TEM image of GNS@AgNPs, (**c**) Partially enlarged view of (**b**). The lattice constant d of silver was 0.23 nm. And (d) TEM image of MWCNT@AgNPs. The silver lattice diffraction pattern as shown in the inset of (**d**). SEM images of (**e**) (GNS-CNTs)@AgNPs/PVA film, (**f**) MWCNT/PVA, (**g**) GNS/PVA, (**h**) (GNS-MWCNT)/PVA, and (**i**) partially enlarged view of 20 vol% (GNS-MWCNTs)@AgNPs/PVA. Particle average size of synthesized silver was about 20 nm, thickness and surface area of 2D GNS were about 5–9 nm and 25 μm^2, and MWCNTs possessed 40 nm in diameter and 1–2 μm in average length.

Both the volume and surface resistivities of the (GNS-MWCNT)@AgNPs/PVA composite films with different volume fractions of fillers (0, 5%, 10%, 15%, and 20%) were measured using the 2-point method at room temperature. The results are presented in Figure 3. As shown in Figure 3, the volume and surface resistance of the films decreased gradually with increased nanofiller loading. The results suggested that although the volume resistance and surface resistance of the films decreased gradually, they were within the range of accepted properties for electronic packaging and/or electrical insulation material applications [26,43–48]. The inset of Figure 3 shows the effects of four fillers on the flexural strength of the composites compared to the pure PVA matrix. The maximum flexural strength of the (GNS-MWCNT)@AgNPs/PVA composite with 20 vol% fillers loading increased to 131.0 MPa, which was increased by 47.2% compared to the pure PVA matrix (89.0 MPa). Appropriate fillers with surface modification could effectively transfer stress and facilitate stress relaxation under external forces, finally leading to improve the flexural strength of the composites.

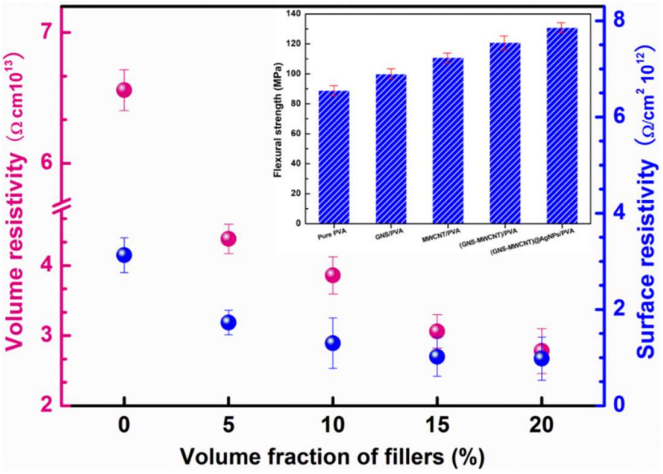

Figure 3. Effect of filler loading on volume resistance and surface resistance of (GNS-MWCNT)@AgNPs/PVA nanocomposite films, and effects of different fillers on the flexural strength of composites compared with that of pure PVA matrix (inset).

Table 1. Glass transition temperatures, coefficient of thermal expansion, and thermal decomposition temperature of pure PVA and its composites filled with GNS, MWCNT, and (GNS-MWCNT)@AgNPs at 5%, 10%, 15%, and 20% fillers loading.

Sample	Content (vol%)	T_g [a] (°C)	CTE [b] (ppm/°C)	$T_{d5\%}$ [c] (°C)
Pure PVA	0	208.2 ± 4.4	40.5 ± 1.2	517.3 ± 10.4
GNS/PVA	5	211.4 ± 6.3	41.1 ± 1.5	525.6 ± 11.2
	10	211.6 ± 4.2	39.6 ± 2.4	517.5 ± 9.80
	15	211.8 ± 5.1	38.4 ± 2.3	528.2 ± 10.8
	20	212.2 ± 4.3	38.2 ± 2.1	527.3 ± 10.3
MWCNT/PVA	5	210.3 ± 5.5	40.2 ± 3.0	514.3 ± 9.90
	10	211.5 ± 4.4	39.1 ± 2.7	513.5 ± 11.2
	15	212.1 ± 4.1	38.7 ± 2.6	528.2 ± 10.8
	20	212.3 ± 5.6	38.2 ± 2.7	522.9 ± 12.3
(GNS-MWCNT)@AgNPs /PVA	5	210.4 ± 6.1	39.8 ± 2.3	518.2 ± 11.1
	10	210.6 ± 4.8	39.3 ± 3.2	519.4 ± 10.2
	15	211.1 ± 6.5	38.7 ± 3.2	524.8 ± 10.9
	20	212.4 ± 5.5	38.2 ± 2.5	526.2 ± 11.4

T_g [a], glass transition temperature. CTE [b], coefficient of thermal expansion, measured using TMA determined over a range of 100–200 °C. $T_{d5\%}$ [c], thermal decomposition temperature at 5% weight loss as determined using TGA.

The thermal conductivities of composites greatly depended on the properties of polymers and fillers, such as their content, components, and surface treatment of fillers [49–54]. Comparison charts of thermal conductivities and their enhancements for GNS/PVA, MWCNT/PVA, (GNS-MWCNT)/PVA, and (GNS-MWCNT)@AgNPs/PVA composite films with different nanofillers are shown in Figure 4. As shown in Figure 4a, the thermal conductivity of the pure PVA was about 0.178 W/mK. The thermal conductivities of the aforementioned four composite films increased with the increase in filler loading. Further, the thermal conductivity of (GNS-MWCNT)@AgNPs/PVA was higher than that of the other three films and reached the highest value of 12.3W/mK at 20% filler loading. The efficiency of fillers in thermally conductive materials were characterized by thermal conductivity enhancement, which was defined by the following equation [48]:

$$\eta\ (\%) = \frac{K_c - K_m}{K_m} \times 100 \quad (2)$$

Preprints (www.preprints.org) | NOT PEER-REVIEWED | Posted: 25 October 2018 doi:10.20944/preprints201808.0290.v2

Peer-reviewed version available at Crystals 2018, 8, 398; doi:10.3390/cryst8110398

where K_c represents the thermal conductivity of the composite, and K_m is the thermal conductivity of the matrix material. As shown in Figure 4b, the enhanced matrix thermal conductivity was always larger than that for GNS/PVA, MWCNT/PVA, and (GNS-MWCNT)/PVA composite films at 5%, 10%, 15%, and 20% filler loading, respectively. The maximum thermal conductivity of (GNS-MWCNT)@AgNPs/PVA composite with 20% filler low loading increased to 12.3 W/mK, representing an approximate enhancement of 6810.1 times, compared to the used pure PVA matrix. Graphene nanosheets could be considered as a 2D materials, multiwalled carbon nanotube could be considered as a one-dimensional material, and GNS@AgNPs and MWCNT@AgNPs could be considered as 2@0 and 1@0 coated structures. Compared to GNS/PVA and MWCNT/PVA films, silver nanoparticles coated with GNS and MWCNT provided an effective bond between fillers and PVA polymer, enabling effective thermal conductivity, compared to the films without silver nanoparticles at the same filler loading. Hence, it was fair to conclude that multidimensional structure fillers improved the thermal conductivity of polymer matrix composite materials compared to the single-dimensional structure fillers [28].

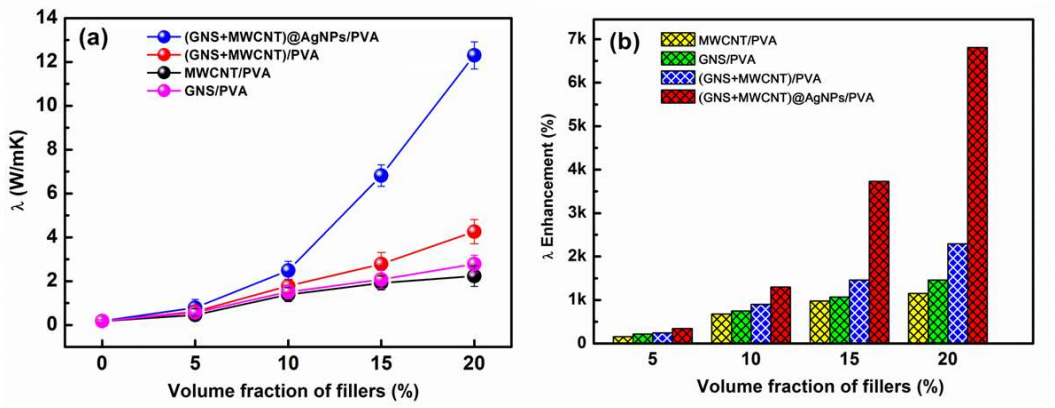

Figure 4. Thermal conductivity λ (**a**) and thermal conductivity enhancement (**b**) of GNS/PVA, MWCNT/PVA, (GNS-MWCNT)/PVA, and (GNS-MWCNT)@AgNPs/PVA nanocomposite films with different volume fractions of fillers.

Printability and thermal expansion are important parameters of TIM when applied between the surfaces of heat-generating devices and heat sink in the advanced microelectronics packaging technology. The CPU cooling of the desktop computer was investigated using TIM for heat dissipation, as shown in Figure 5a. The (GNS-MWCNT)@AgNPs/PVA TIM was applied between the

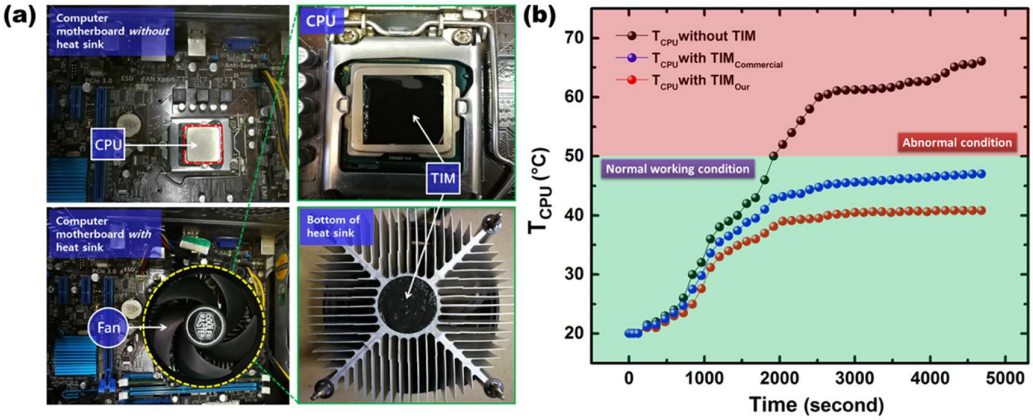

Figure 5. Changes in computer CPU cooling with the temperature of (GNS-MWCNT)@AgNPs/PVA TIM and a commercial TIM were investigated. An optical image of the coating-printed (GNS-MWCNT)@AgNPs/PVA TIM is provided in the inset of (**a**). Optical images of a CPU on a motherboard before and after the installation of a heat sink with a fan. T-type thermocouples were employed to

measure the temperatures of the CPU. Temperature (T_{CPU}) profiles were investigated with two kinds of TIMs and without TIM between the CPU and heat sink. (**b**) Experimental data of T_{CPU} with TIMs under normal working conditions were also compared with the data of T_{CPU} without TIM.

CPU and a heat sink and cured at 120 °C for 5 h. A cooler master fan was attached at the top of the heat sink. The surface temperature of the CPU (T_{CPU}) was measured using T-type thermocouples at room temperature. A commercial TIM (ARCTIC MX-4, Shenzhen, China $\lambda = 8.5$ W/mK) was chosen as a comparison. As shown in Figure 5b, T_{CPU} without and with two kinds of TIMs were room temperature initially, which increased gradually with the increase in time. T_{CPU} without TIM was more than 50 °C after about 2000 s and increased with time, gradually into the abnormal conditions (more than 50 °C). However, T_{CPU} with two kinds of TIMs were always normal, a better heat dissipation performance was obtained by the (GNS-MWCNT)@AgNPs/PVA TIM compared with that of commercial TIM. The highest T_{CPU} of (GNS-MWCNT)@AgNPs/PVA TIM was only about 40°C. Hence, it was evident that using TIM obtained could more effectively reduce the redundant heat compared with CPU without TIM and commercial TIM.

4. Conclusions

In summary, silver-functionalized GNS and MWCNT composites with excellent thermal properties were developed in this study. The effects of composites on the interfacial structure and properties of the composites were identified, and the microstructures and properties of the composites were studied as a function of the volume fraction of fillers. An ultrahigh thermal conductivity of 12.3 W/mK for polymer matrix composites was obtained, which was enhanced by approximately 69.1 times compared to the PVA matrix. Further, these composites displayed more competitive thermal conductivities compared to the untreated fillers/PVA composites, and more effectively reduced the redundant heat, compared to CPU without TIM and commercial TIM. This technique provides insight into designing thermally conductive polymer composites, highlighting the potential for its use in the next-generation electronic packaging.

Authors Contributions: Y.Z. and X.Z. designed and performed all experiments. Y.Z. and F.W. analyzed the data and wrote the manuscript. All authors have read and approved the final manuscript.

Funding: This study was supported by the National Natural Science Foundation of China (51707159), the Natural Science Foundation of Shannxi Province (2017JM5073), the State Key Laboratory of Electrical Insulation and Power Equipment (EIPE17205), and the Fundamental Research Funds for the Central Universities (3102017zy047).

Conflicts of Interest: The authors declare no conflicts of interest.

References

1. De Volder, M.F.L.; Tawfick, S.H.; Baughman, R.H.; Hart, A.J. Carbon nanotubes: Present and future commercial applications. *Science* **2013**, *339*, 535–539.
2. Chen, J.; Huang, X.; Zhu, Y.; Jiang, P. Cellulose nanofiber supported 3D interconnected BN nanosheets for epoxy nanocomposites with ultrahigh thermal management capability. *Adv. Funct. Mater.* **2017**, *27*, 1604754.
3. Fu, Z.; Chen, K.; Li, L.; Zhao, F.; Wang, Y.; Wang, M.; Shen, Y.; Cui, H.; Liu, D.; Guo, X. Spherical and spindle-like abamectin-loaded nanoparticles by flash nanoprecipitation for southern root-knot nematode control: Preparation and characterization. *Nanomaterials* **2018**, *8*, 449.
4. Wang, G.; Yu, D.; Kelkar, A.D.; Zhang, L. Electrospun nanofiber: Emerging reinforcing filler in polymer matrix composite materials. *Prog. Polym. Sci.* **2017**, *75*, 73–107.
5. Wang, Y.; Wang, A.; Wang, C.; Cui, B.; Sun, C.; Zhao, X.; Zeng, Z.; Shen, Y.; Gao, F.; Liu, G.; et al. Synthesis and characterization of emamectin-benzoate slow-release microspheres with different surfactants. *Sci. Rep.* **2017**, *7*, 12761.
6. Shen, Y.; Wang, Y.; Zhao, X.; Sun, C.; Cui, B.; Gao, F.; Zeng, Z.; Cui, H. Preparation and physicochemical characteristics of thermo-responsive emamectin benzoate microcapsules. *Polymers* **2017**, *9*, 418.

7. Zhou, Y.; Yao, Y.; Chen, C.; Moon, K.; Wang, H.; Wong, C.P. The use of polyimide-modified aluminum nitride fillers in AlN@PI/Epoxy composites with enhanced thermal conductivity for electronic encapsulation. *Sci. Rep.* **2014**, *4*, 4779.
8. Pan, C.; Zhang, J.; Kou, K.; Zhang, Y.; Wu, G. Investigation of the through-plane thermal conductivity of polymer composites with in-plane oriented hexagonal boron nitride. *Int. J. Heat Mass Transf.* **2018**, *120*, 1–8.
9. Saadah, M.; Hernandez, E.; Balandin, A. Thermal management of concentrated multi-junction solar cells with graphene-enhanced thermal interface materials. *Appl. Sci.* **2017**, *7*, 589.
10. Li, Z.; Li, Z.; Sun, S.; Zheng, D.; Wang, H.; Tian, H.; Yang, H.; Bai, X.; Li, J. Direct observation of inner-layer inward contractions of multiwalled boron nitride nanotubes upon in situ heating. *Nanomaterials* **2018**, *8*, 86.
11. Wang, J.; Wang, H.; Cao, D.; Lu, X.; Han, X.; Niu, C. Epitaxial growth of urchin-like $CoSe_2$ nanorods from electrospun co-embedded porous carbon nanofibers and their superior lithium storage properties. *Part. Part. Syst. Charact.* **2017**, *34*, 1700185.
12. Feng, A.; Jia, Z.; Yu, Q.; Zhang, H.; Wu, G. Preparation and characterization of carbon nanotubes/carbon fiber/phenolic composites on mechanical and thermal conductivity properties. *NANO* **2018**, *13*, 1850037.
13. Renteria, J.; Legedza, S.; Salgado, R.; Balandin, M.P.; Ramirez, S.; Saadah, M.; Kargar, F.; Balandin, A.A. Magnetically-functionalized self-aligning graphene fillers for high-efficiency thermal management applications. *Mater. Des.* **2015**, *88*, 214–221.
14. Cavallaro, G.; Danilushkina, A.A.; Evtugyn, V.G.; Lazzara, G.; Milioto, S.; Parisi, F.; Parisi, E.V.; Fakhrullin, R.F. Halloysite nanotubes: Controlled access and release by smart gates. *Nanomaterials* **2017**, *7*, 199.
15. Zhou, Y.C.; Wang, H.; Wang, L.; Yu, K.; Lin, Z.D.; Bai, Y.Y. Fabrication and characterization of aluminum nitride polymer matrix composites with high thermal conductivity and low dielectric constant for electronic packaging. *Mater. Sci. Eng. B* **2012,** *177*,892–896.
16. Zhou, Y.C.; Wang, H.; Xiang, F.; Zhang, H.; Yu, K.; Chen, L. A poly(vinylidene fluoride) composite with added self-passivated microaluminum and nanoaluminum particles for enhanced thermal conductivity. *Appl. Phys. Lett.* **2011**, *98*, 182906.
17. Yu, L.; Park, J.; Lim, Y.; Lee, C.; Shin, K.; Moon, H.; Yang, C.; Lee, Y.; Han, J. Carbon hybrid fillers composed of carbon nanotubes directly grown on graphene nanoplatelets for effective thermal conductivity in epoxy composites. *Nanotechnology* **2013**, *24*, 155604.
18. Terao, T.; Zhi, C.; Bando, Y.; Mitome, M.; Tang, C.; Golberg, D. Alignment of boron nitride nanotubes in polymeric composite films for thermal conductivity improvement. *J. Phys. Chem. C* **2010**, *114*, 4340–4344.
19. Zhao, Y.; Zhang, Y.; Bai, S. High thermal conductivity of flexible polymer composites due to synergistic effect of multilayer graphene flakes and graphene foam. *Compos. Part A* **2016**, *85*, 148–155.
20. Wang, F.; Drzal, L.T.; Qin, Y.; Huang, Z. Enhancement of fracture toughness, mechanical and thermal properties of rubber/epoxy composites by incorporation of graphene nanoplatelets. *Compos. Part A* **2016**, *87*, 10–22.
21. Shenogin, S.; Bodapati, A.; Xue, L.; Ozisik, R.; Keblinski, P. Effect of chemical functionalization on thermal transport of carbon nanotube composites. *Appl. Phys. Lett.* **2004**, *85*, 2229–2231.
22. Guo, K.; Hu, Z.; Song, H.; Du, X.; Zhong, L.; Chen, X. Low-density graphene/carbon composite aerogels prepared at ambient pressure with high mechanical strength and low thermal conductivity. *RSC Adv.* **2015**, *5*, 5197–5204.
23. Fan, Z.; Tng, D.Z.Y.; Nguyen, S.T.; Feng, J.D.; Lin, C.F.; Xiao, P.F.; Lu, L.; Duong, H.M. Morphology effects on electrical and thermal properties of binderless graphene aerogels. *Chem. Phys. Lett.* **2013**, *561*, 92–96.
24. Cheng, Y.; Zhou, S.; Hu, P.; Zhao, G.; Li, Y.; Zhang, X.; Han, W. Enhanced mechanical, thermal, and electric properties of graphene aerogels via supercritical ethanol drying and high-temperature thermal reduction. *Sci. Rep.* **2017**, *7*, 1439.
25. Gong, F.; Bui, K.; Papavassiliou, D.V.; Duong, H.M. Thermal transport phenomena and limitations in heterogeneous polymer composites containing carbon nanotubes and inorganic nanoparticles. *Carbon* **2014**, *78*, 305–316.
26. Deng, Y.; Li, J.H.; Nian, H.G.; Li, Y.L.; Yin, X.P. Design and preparation of shape-stabilized composite phase change material with high thermal reliability via encapsulating polyethylene glycol into flower-like TiO_2, nanostructure for thermal energy storage. *Appl. Therm. Eng.* **2017**, *114*, 328–336.

27. Roy, A.K.; Farmer, B.L.; Varshney, V.; Sihn, S.; Lee, J.; Ganguli, S. Importance of interfaces in governing thermal transport in composite materials: Modeling and experimental perspectives. *ACS Appl. Mater. Interfaces* **2012**, *4*, 545–563.
28. Zhou, Y.; Liu, F.; Wang, H. Novel organic-inorganic composites with high thermal conductivity for electronic packaging applications: A key issue review. *Polym. Compos.* **2017**, *38*, 803–813.
29. Safari, A.; Saidur, R.; Sulaiman, F.A.; Xu, Y.; Dong, J. A review on supercooling of Phase Change Materials in thermal energy storage systems. Renew. *Sustain. Energy Rev.* **2016**, *70*, 905–919.
30. Zhou, Y.; Liu, F. High-performance polyimide nanocomposites with core-shell AgNWs@BN for electronic packagings. *Appl. Phys. Lett.* **2016**, *109*, 082901.
31. Su, J.F.; Wang, X.Y.; Han, S.; Zhang, X.L.; Guo, Y.D.; Wang, Y.Y.; Tan, Y.Q. Preparation and physicochemical properties of microcapsules containing phase change material with graphene/organic hybrid structure shells. *J. Mater. Chem. A* **2017**, *5*, 23937–23951.
32. Cai, Y.; Sun, G.; Liu, M.; Zhang, J.; Wang, Q.; Wei, Q. Fabrication and characterization of capric-lauric-palmitic acid/electrospun SiO_2, nanofibers composite as form-stable phase change material for thermal energy storage/retrieval. *Sol. Energy* **2015**, *118*, 87–95.
33. Chun, K.Y.; Oh, Y.; Rho, J.; Ahn, J.H.; Kim, Y.J.; Choi, H.; Baik, S. Highly conductive, printable and stretchable composite films of carbon nanotubes and silver. *Nat. Nanotechnol.* **2010**, *5*, 853–857.
34. Zhang, X.; Sun, D.; Li, Y.; Lee, G.-H.; Cui, X.; Chenet, D.; You, Y.; Heinz, T.F.; Hone, J.C. Measuremen of Lateral and Interfacial Thermal Conductivity of Single- and Bilayer MoS_2 and $MoSe_2$ Using Refined Optothermal Raman Technique. *ACS Appl. Mater. Interfaces* **2015**, *7*, 25923–25929.
35. Zhao, Y.J.; Min, X.; Huang, Z.H.; Fang, M.H. Honeycomb-like structured biological porous carbon encapsulating PEG: A shape-stable phase change material with enhanced thermal conductivity for thermal energy storage. *Energy Build.* **2017**, *158*, 1049–1062.
36. Ibrahim, N.I.; Al-Sulaiman, F.A.; Rahman, S.; Yilbas, B.S.; Sahin, A.Z. Heat transfer enhancement of phase change materials for thermal energy storage applications: A critical review. Renew. *Sustain. Energy Rev.* **2017**, *74*, 26–50.
37. Lv, P.Z.; Liu, C.Z.; Rao, Z.H. Review on clay mineral-based form-stable phase change materials: Preparation, characterization and applications. Renew. *Sustain. Energy Rev.* **2016**, *68*, 707–726.
38. Bauld, R.; Choi, D.Y.W.; Bazylewski, P.; Divigalpitiya, R.; Fanchini, G. Thermo-optical characterization and thermal properties of graphene-polymer composites: A review. *J. Mater. Chem. C* **2018**, *6*, 2901–2914.
39. Zhang, L.; Yang, W.B.; Jiang, Z.N.; He, F.F.; Zhang, K.; Fan, J.H.; Wu, J.Y. Graphene oxide-modified microencapsulated phase change materials with high encapsulation capacity and enhanced leakage-prevention performance. *Appl. Energy* **2017**, *197*, 354–363.
40. Yuan, H.; Wang, Y.; Li, T.; Ma, P.M.; Zhang, S.W.; Du, M.L.; Chen, M.Q.; Dong, W.F.; Ming, W.H. Highly thermal conductive and electrically insulating polymer composites based on polydopamine-coated copper nanowire. *Compos. Sci. Technol.* **2018**, *164*, 153–159.
41. Shtein, M.; Nadiv, R.; Buzaglo, M.; Kahil, K.; Regev, O. Thermally conductive grapheme polymer composites: Size, percolation, and synergy effects. *Chem. Mater.* **2015**, *27*, 2100–2106.
42. Dai, W.; Yu, J.H.; Wang, Y.; Song, Y.Z.; Alam, F.E.; Nishimura, K.; Lin, C.T.; Jiang, N. Enhanced thermal conductivity for polyimide composites with a three-dimensional silicon carbide nanowire@graphene sheets filler. *J. Mater. Chem. A* **2015**, *3*, 4884–4891.
43. Su, J.F.; Wang, L.X.; Ren, L.; Huang, Z. Mechanical properties and thermal stability of double-shell thermal energy storage microcapsules. *J. Appl. Polym. Sci.* **2007**, *103*, 1295–1302.
44. Wang, J.J.; Yang, M.; Lu, Y.F.; Jin, Z.K.; Tan, L.; Gao, H.Y.; Fan, W.J.; Wang, G. Surface functionalization engineering driven crystallization behavior of polyethylene glycol confined in mesoporous silica for shape-stabilized phase change materials. *Nano Energy* **2016**, *19*, 78–87.
45. Wang, F.F.; Zeng, X.L.; Yao, Y.M.; Sun, R.; Xu, J.B.; Wong, C.P. Silver nanoparticle-deposited boron nitride nanosheets as fillers for polymeric composites with high thermal conductivity. *Sci. Rep.* **2016**, *6*, 19394.
46. Zhuang, X.; Zhou, Y.C.; Liu, F. A novel 3D sandwich structure of hybrid graphite nanosheets and silver nanowires as fillers for improved thermal conductivity. *Mater. Res. Express* **2017**, *4*, 015018.
47. Zhou, Y.C.; Luo, Z.P.; Zhuang, X.; Liu, F. Multilayer-structured high-performance nanocomposites based on a combination of silver nanoparticles and nanowires. *Mater. Lett.* **2016**, *182*, 323–327.
48. Bao, R.; Yan, S.L.; Wang, R.G.; Li, Y.J. Experimental and theoretical studies on the adjustable thermal properties of epoxy composites with silver-plated short fiberglass. *J. Appl. Polym. Sci.* **2017**, *134*, 45555.

49. Viana, S.T.; Scariot, V.K.; Provensi, A.; Barra, G.M.O.; Barbosa, J.R. Fabrication and thermal analysis of epoxy resin-carbon fiber fabric composite plate-coil heat exchangers. *Appl. Therm. Eng.* **2017**, *127*, 1451–1460.
50. Dong, Q.; Yoon, S.J.; Zhang, J.; Yoon, H.S.; Kim, T.G. Research on Thermal Conductivity of Electrospun Polyacrilonitrile-Multi-Walled Carbon Nanotubes Composite Carbon Nanofiber Papers. *J. Nanosci. Nanotechnol.* **2018**, *18*, 7095–7099.
51. Govindara, A.; Satishkumar, B.C.; Nath, M.; Rao, C. Metal nanowires and intercalated metal layers in single-walled carbon nanotube bundles. *Chem. Mater.* **2000**, *12*, 202–205.
52. Sadej, M.; Gojzewski, H.; Gajewski, P.; Vancso, G.J.; Andrzejewska, E. Photocurable acrylate-based composites with enhanced thermal conductivity containing boron and silicon nitrides. *Express Polym. Lett.* **2018**, *12*, 790–807.
53. Xu, Y.J.; Ren, S.X.; Zhang, W.H. Thermal conductivities of plain woven C/SiC composite: Micromechanical model considering PyC interphase thermal conductance and manufacture-induced voids. *Compos. Struct.* **2018**, *193*, 212–223.
54. Mechrez, G.; Suckeveriene, R.Y.; Zelikman, E.; Rosen, J.; Ariel-Sternberg, N.; Cohen, R.; Narkis, M.; Segal, E. Highly-Tunable Polymer/Carbon Nanotubes Systems: Preserving Dispersion Architecture in Solid Composites via Rapid Microfiltration. *ACS Macro Lett.* **2012**, *1*, 848–852.